

Multiferroic behavior in EuTiO₃ films constrained by symmetryP. J. Ryan,^{1,9,*} G. E. Sterbinsky,¹ Y. Choi,¹ J. C. Woicik,² Leyi Zhu,³ J. S. Jiang,³ J.-H. Lee,⁴ D. G. Schlom,^{4,5} T. Birol,⁶ S. D. Brown,⁷ P. B. J. Thompson,⁷ P. S. Normile,⁸ J. Lang,¹ and J.-W. Kim¹¹*Advanced Photon Source, Argonne National Laboratory, Argonne, Illinois 60439, USA*²*National Institute of Standards and Technology, Gaithersburg, Maryland 20899, USA*³*Materials Science Division, Argonne National Laboratory, Argonne, Illinois 60439, USA*⁴*Department of Materials Science and Engineering Cornell University, Ithaca, New York 14853, USA*⁵*Kavli Institute at Cornell for Nanoscale Science, Ithaca, New York 14853, USA*⁶*Department of Chemical Engineering and Materials Science, 421 Washington Avenue, SE, Minneapolis, Minnesota 55455-0132, USA*⁷*Department of Physics, University of Liverpool, Liverpool L69 3BX, United Kingdom*⁸*Departamento de Física Aplicada and Instituto Regional de Investigación Científica Aplicada (IRICA), Universidad de Castilla-La Mancha, 13071 Ciudad Real, Spain*⁹*School of Physical Sciences, Dublin City University, Dublin 9, Ireland*

(Received 25 April 2019; revised manuscript received 10 February 2020; accepted 1 May 2020; published 29 May 2020)

We have elucidated the spin, lattice, charge, and orbital coupling mechanism underlying the multiferroic character in tensile-strained EuTiO₃ films. Symmetry determined by oxygen octahedral tilting shapes the hybridization between the Eu 4*f* and the Ti 3*d* orbitals, and this inhibits predicted Ti displacement proper ferroelectricity. Instead, phonon softening emerges at low temperatures within the pseudocube (110) plane, orthogonal to the anticipated ferroelectric polarization symmetry. Additionally, the magnetic anisotropy is determined by orbital distortion through hybridization between the Ti 3*d* and the typically isotropic Eu²⁺ 4*f* states. This unique scenario demonstrates the critical role symmetry plays in the coupling of order parameters defining multiferroic behavior.

DOI: [10.1103/PhysRevB.101.180409](https://doi.org/10.1103/PhysRevB.101.180409)

As we uncover the fundamental principles of strong magnetoelectric coupling, the intricate connections among multiple order parameters including spin, lattice, orbital, and charge often manifest as anomalous and intriguing physical phenomena [1,2]. An interesting example demonstrating multiple parameter couplings is EuTiO₃ (ETO), which has been considered a parent candidate to explore multiferroic quantum criticality [3]. In bulk, it is a quantum paraelectric antiferromagnet (AFM) displaying strong magnetodielectric behavior at the onset of its *G*-type AFM ordering [4,5]. As illustrated in Fig. 1, ETO has coexisting ferromagnetic (FM) and AFM interactions described in the context of different pathways between Eu ions [6]. Under tensile strain, ETO thin films have demonstrated FM order, which was predicted and shown to be coupled to ferroelectric order induced by Ti noncentral symmetry [7,8].

Coexisting competing ferromagnetic and antiferromagnetic interactions coupled with a large and diverging dielectric constant at low temperatures indicative of proximity to a ferroelectric transition make ETO a strong parent candidate for potential multiferroic quantum critical behavior [3]. A combination of chemical pressure, magnetic dilution, and biaxial strain is theoretically predicted to induce both magnetic and ferroelectric quantum criticalities separately and potentially engineer both behaviors to converge at the same point in

phase space [3,9]. However, in order to explore such exotic phenomena, knowing the behavior of and coupling between the order parameters of the parent compound is crucial. In particular, the role symmetry plays in shaping the orbital states of both Eu and Ti, which determine the magnetic and electric parameters, respectively, will ultimately determine how both quantum critical points behave and possibly interact.

In this Rapid Communication, we present a study of the relationship between the electric and the magnetic polarizations with structural symmetry as determined by the octahedral (O_h) rotation pattern in tensile-strained ETO epitaxial thin films. We explain how the FM order exhibits uniaxial anisotropy and remarkably why the system resists breaking central symmetry. The oxygen O_h tilt pattern alters the orbital topology consisting of Eu (4*f*), O (2*p*), and Ti (3*d*) bands. In doing so, the tilt differentiates between the (110)_{pc} and the ($\bar{1}10$)_{pc} planes generating an azimuthally dependent interorbital distortion of the Eu 4*f* states. In the *d*⁰ titanite perovskites, the oxygen O_h tilt would generally lead to central symmetry breaking along the O_h rotational vector [10,11]. Instead, a significant softening of the Slater mode is observed within the plane orthogonal to the anticipated FE polarization direction [10]. Polarized x-ray absorption near edge spectroscopy at the Ti *K* absorption transition shows the correlated Ti phonon softening at low temperatures on this plane where crystal symmetry forbids central symmetry breaking. In addition, employing resonant x-ray magnetic scattering, we relate both spin and phonon anisotropies with structural symmetry. In aggregate, these

*Corresponding author: pryan@anl.gov

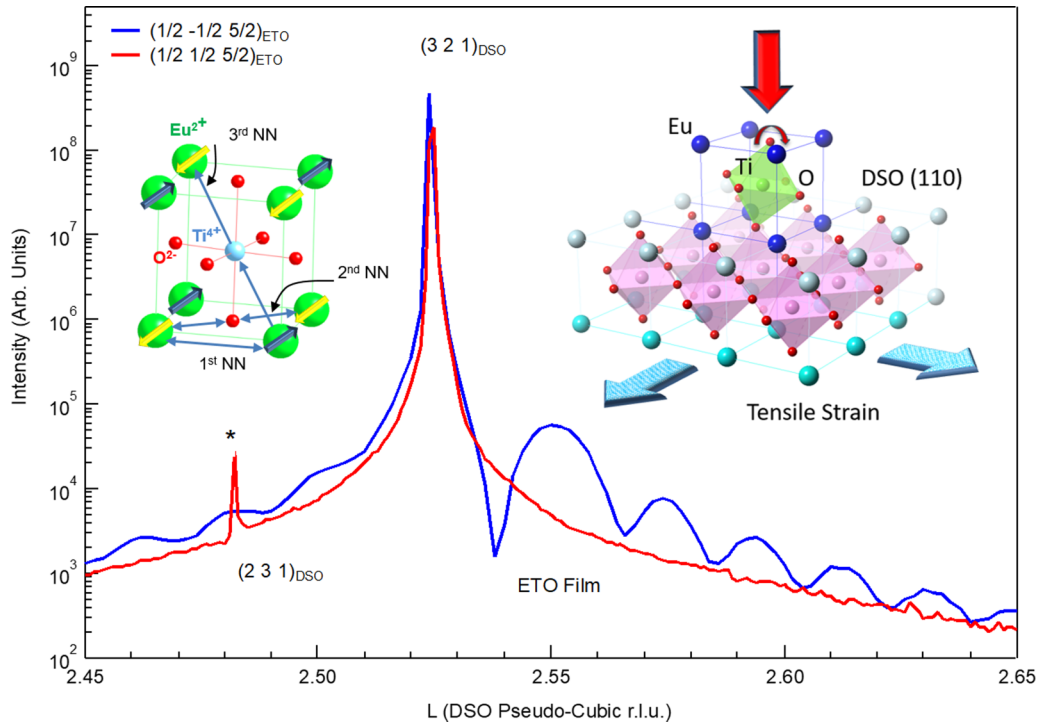


FIG. 1. Reciprocal space scans (along the L direction) of half order reflections resulting from the oxygen octahedral tilt pattern. Absence of the half order $(\frac{1}{2} \frac{1}{2} \frac{5}{2})$ indicates that the film has a single-type tilt domain. Cartoons illustrating (left) the ETO pseudocubic unit cell showing *G*-AFM order with all three coexisting spin-ordering interactions and (right) the biaxial strain and single oxygen-related tilt pattern imposed by the DSO (110) substrate.

measurements reveal the relative oriented coupling behavior of the symmetry with spin, lattice, and orbital parameters of the film.

The ETO epitaxial 25-nm film, grown by reactive molecular-beam epitaxy, is fully constrained to the DyScO_3 (DSO)(110)_o (orthorhombic) substrate [8]. The orthorhombic symmetry of the DSO substrate induces a single O_h rotation pattern in the ETO film as identified by x-ray-diffraction measurements of half order reflections illustrated in Fig. 1 [12]. As we discussed previously [11], the tensile strain leads to the metastable state, *Imma* ($a^-a^-c^0$) [12] with symmetry breaking between [110] and $[\bar{1}10]$ through O_h tilting. There are two possible tilt domains, along the [110] and $[\bar{1}10]$ directions. The half order $(\frac{1}{2} \frac{1}{2} L/2)$ reflections are allowed for the [110] O_h tilt domain but not for the $[\bar{1}10]$ domain. The absence of $(\frac{1}{2} \frac{1}{2} \frac{5}{2})$ reflection, therefore, verifies the single tilt pattern.

The Ti atom is of particular importance to the electronic band characteristics of this material and considered responsible for ferroelectricity in the titanate-perovskite systems [13,14]. Additionally, it is a key element underlying the multiferroic, magnetoelectric, and possible multiferroic-quantum critical characteristics of EuTiO_3 [3,5–10] as it mediates the *G*-type AFM superexchange mechanism between the Eu (4*f*) states via the Ti 3*d* orbitals [15]. In fact, the localized 4*f* spins hybridize with the Eu (5*d*), Ti (3*d*), and O (2*p*) states, illustrating the potential of strong interatomic coupling phenomena [15]. To investigate the configuration of Ti electronic states, we employed linear-polarized x-ray absorption spectroscopy at the Ti *K* edge (Fig. 2). The *K* edge is dominated by

the allowed dipole transition from 1*s* to 4*p* orbitals whereas the 1*s* to 3*d* transition is forbidden. However, *p* character is introduced to the 3*d* states through orbital hybridization that occurs with static or dynamic symmetry breaking, which gives rise to preedge features. For this reason, the preedge e_g intensity is proportional to the square of the component of the Ti displacement along the incoming beam polarization ([16–18]).

In Fig. 2(b), the inset cartoon illustrates the grazing incidence experimental geometry. The lack of an anomalously large change in the intensity of the preedge e_g peak with temperature suggests that there is not static central symmetry breaking. This, then, rules out the picture of simple proper FE behavior via a *B*-site displacement. However, in Fig. 2, there are subtle but significant changes to the e_g intensity. These effects relate to modulus changes in the phonon modes [19]. Figure 2(b) presents a comparison of the e_g intensity between incoming photon polarizations *e* along the film in-plane [1 0 0] and out-of-plane [0 0 1] directions at room temperature and at 15 K. At 15 K, the reversal of the in/out-of-plane e_g intensity demonstrates an unexpected increase in the modulus of the Ti position in the direction normal to the film as illustrated in the cartoon model Fig. 2(c) whereas the in-plane phonon modulus decreases with temperature.

Similar in-plane azimuthal comparisons are shown in Fig. 2(d). The preedge e_g intensity change derives primarily from a temperature effect, and the intensities are indistinguishable between $e||[110]$ and $e||[\bar{1}10]$. However, at 15 K, the intensity of $e||[\bar{1}10]$ increases and is attributed to a phonon softening along this direction [Fig. 2(e)], whereas, along the

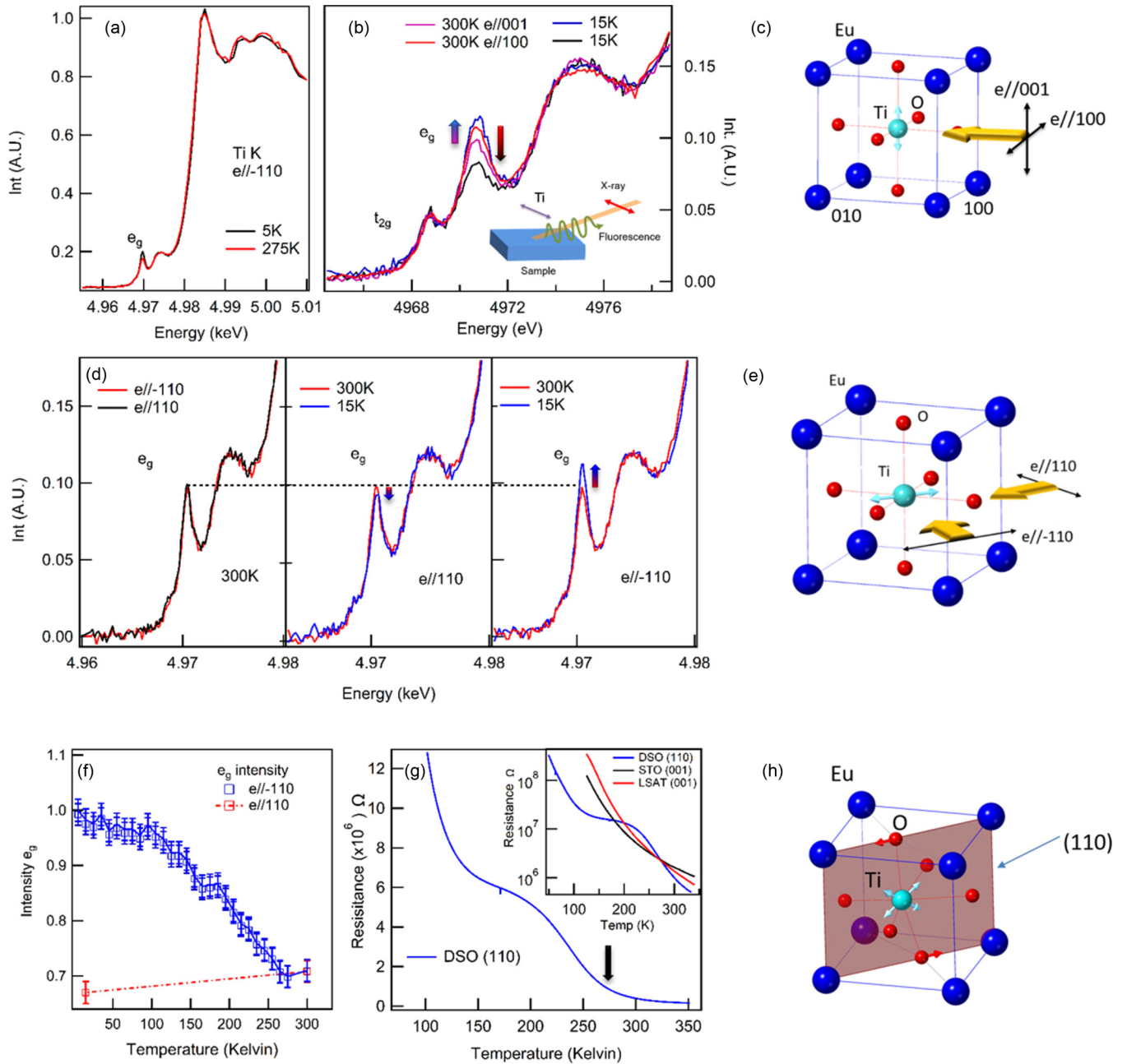


FIG. 2. (a) Ti K -edge near-edge spectra with linear polarization at 5 and 275 K. (b) Expanded plots of the spectral intensities of the e_g preedge peak contrasting the temperature dependence of polarization parallel to both in-plane [100] and out-of-plane [001] as depicted in the inset. (c) Cartoon illustration of the relative incident polarization (yellow arrows) with low-temperature phonon softening effect along [001] (cyan arrow). (d) Azimuthal-temperature dependence of e_g preedge intensity along both $e||[110]$ and $e||[\bar{1}10]$. (e) Cartoon displaying the relative incident geometries with the arrow indicating increased softening. (f) Temperature dependence of the e_g preedge intensity with the polarization along the [110] and $[\bar{1}10]$. (g) Temperature dependence of the in-plane film resistance. The inset shows the comparison between other strain states. (h) Cartoon showing the aggregate relative orientation of Ti phonon softening along the cube diagonal with respect to the oxygen tilting within the (110) plane.

[110] direction, the anticipated decrease is observed. Having an increased e_g intensity both along [001] and $[\bar{1}10]$ suggests a cube diagonal $[\bar{1}11]$ (or $[1\bar{1}1]$) net softening phenomenon. The temperature dependence is very similar to the published second-harmonic generation results [8]. An uptick in resistance is measured at roughly the same temperature [Fig. 2(g)] as the e_g intensity in Fig. 2(f). Recent density functional the-

ory (DFT) calculations propose net band-gap widening with increasing O $2p$ and Ti $3d$ orbital mixing in biaxially strained SrTiO_3 films whereby lowering the symmetry through ferroic distortions by either oxygen O_h rotation or Ti displacement, the conduction (O $2p$) and valence states (Ti $3d$) are allowed to mix [20]. Thus, effective net charge on the Ti d^0 orbital leads to charge repulsion which emerges as the distinction

between bond phase parity is removed [21]. Although dynamic, the Ti displacement along the cube diagonal widens the gap resulting in a clear uptick in resistance at ~ 270 K. This behavior demonstrates that the band-edge active orbitals Ti ($3d$) and O ($2p$) are tightly coupled and respond to the amplitude of atomic vibrations.

The lack of central symmetry breaking can be understood as the effect of cross-gap hybridization between the empty transition- d (cation) band and the occupied O $2p$ band [19]. Any Ti shift towards the oxygen increases the Ti-O hybridization further increasing the gap between the unoccupied states (higher) and the occupied states (lower) [22]. With Eu hybridization-induced partial occupation of the Ti d state, there is an additional energy cost pushing the unoccupied d states higher. This reduces the probability of FE order [23]. This model also explains the magnetodielectric spin-lattice coupling in ETO [6]. Consequently, a small residual occupation of the Ti ($3d$) orbital due to hybridization inhibits symmetry breaking. Absent the half-filled Eu ($4f$) orbitals, the Ti would likely displace and result in proper FE order [6].

The seminal work of Zhong and Vanderbilt [24] predicted the emergence of Ti FE order in SrTiO₃ under negative isopressure (increased volume) where the Ti displacement displays both in-plane (x, y) and out-of-plane (z) components. Unlike the isotropic negative pressure considered in these calculations, biaxial tensile strain generates an O_h rotation resulting in a symmetry-breaking effect ($a^-a^-c^0$). Covalent bonding between the A -site (Eu) and the oxygen strengthens the O_h rotational order [25] and, subsequently, increases the orbital interaction and hybridization between the Eu ($4f$) and the Ti ($3d$) states [26]. Furthermore, the single O_h tilt pattern in this film differentiates between the interorbital hybridization within the (110) and ($\bar{1}\bar{1}0$) planes. Strictly speaking, the symmetry of the film is $a^-b^-c^0$ rather than $a^-a^-c^0$ because the DSO substrate does not have equal in-plane lattices. Our measurements support that the cube diagonal within the (110) plane is the phonon softening direction, which is not the expected FE polarization direction in this crystallographic group. Symmetrically, the Ti displacement in the tensile environment is anticipated to be along the O_h rotational axis, parallel to the (110), i.e., $a_+^-b_+^-c_+^0$ 8Cm. However, the measured softening occurs along $[\bar{1}\bar{1}1]$ indicative of $a_+^-b_+^-c_+^0$, along which a static displacement is not symmetrically allowed [27].

The symmetry of the hybridization landscape involving all three elements is evidently broken with the O_h unidirectional tilting, affecting the degree of hybridization between the Eu ($4f$) and the Ti ($3d$) within both (110) and ($\bar{1}\bar{1}0$) planes. The instability of the Ti phonon is dependent on the effective charge sharing (hybridization); the more net charge resident on the Ti orbitals, the stiffer the phonon character. The tilting of the O towards the Eu atom repels the charges within the (110) plane, reducing the effective hybridization and allowing a degree of softening. However, full freezing is ultimately inhibited by symmetry.

A simple Ti displacement is unlikely to be the origin of the reported FE behavior [7], however, the A site may, alternatively, be the origin of the polar effect as has been reported driving the improper FE order in NdNiO₃ films [28]. In EuTiO₃, the smaller size of the Eu²⁺ ion compared to typical B -site ferroelectrics, such as BaTiO₃, makes it likely

that Eu is more active in any potential ferroelectricity than Ti. In fact, analysis of neutron-diffraction estimating atomic displacement factors suggests an Eu *delocalization* in bulk single-crystal EuTiO₃ [29]. Interestingly, as a consequence of twinned O_h antiferrodistortive phases, A -site driven antiferroelectric order was calculated in similarly tensile-strained EuTiO₃ [30] and potentially demonstrated in bulk ETO [31].

The tensile strain-induced distortion drives the film into a FM state as previously demonstrated [8]. In addition to Ti displacement [7], DFT describes increasing volume alone as driving this spin transition [32]. Interestingly, the calculated volume for isotropic expansion $\sim 248 \text{ \AA}^3$ agrees well with the measured volume of the tensile-strained state, here, of 243.32 \AA^3 (bulk/unstrained value 238.19 \AA^3). The Eu²⁺ has a spherical $4f^7$ spin configuration, which has nominally zero orbital angular momentum. This leads to an immunity from crystal-field splitting effects that cause single-ion magnetic anisotropy. Instead, multidirectional hybridization of f - d - p [6,15] orbitals driven by oxygen octahedral tilts, can distort the local Eu $4f$ electronic configuration, resulting in magnetic anisotropy. Here, we conclusively link the uniaxial magnetic anisotropy with its easy axis along the $[\bar{1}\bar{1}0]$ with the single symmetry orientation and lattice behavior by employing x-ray magnetic scattering (XRMS) to concomitantly probe the Eu spin relationship to both.

The appearance of an integer reflection (003) at the Eu L_{II} edge in Fig. 3 confirms the FM spin order [33]. In Fig. 3(a), the temperature dependence of magnetic intensity illustrates a T_c of ~ 4.2 K and a critical exponent β of ~ 0.36 . Employing (π - π) polarization analysis at the (003) reflection [inset of Fig. 3(b)], the intensity of both charge and magnetic scattering is comparable, allowing phase interference. Consequently, the measurement is sensitive to the spin direction with respect to the lattice [34]. The difference in energy dependence of the (003) reflection with the applied magnetic field along the $[\bar{1}\bar{1}0]$ and $[1\bar{1}0]$ directions [Fig. 3(b)] illustrates the phase relationship between the magnetic and the charge scattering. Figure 3(c) displays field loops at fixed energy, 7.612 keV at 3.2 K (above the DSO T_N) with the applied field along the $\pm[\bar{1}\bar{1}0]$, $\pm[010]$, and $\sim \pm[110]$ directions. The spins remain within the $[\bar{1}\bar{1}0]$ direction regardless of field direction as illustrated in the Fig. 3(c) inset where the effective magnetic scattering cross section is represented by the green arrow. With Q -vector rotation, the magnetic cross section decreases as the spin easy axis approaches the scattering plane. The loops broaden as the effective field that requires flipping the spins increases. In the Fig. 3(d) inset, the conclusions of all three measurements are presented in schematic form, the oxygen O_h single tilt domain pattern, the uniaxial FM spin anisotropy below T_c 4.2 K, and, finally, the increased in-plane Ti fluctuations below ~ 270 K, each of which coalign within the (110) plane.

To summarize, we have established how a unique symmetry driven by oxygen octahedral tilt shapes the hybridization between the Eu $4f$ and the Ti $3d$ orbitals in ETO films. This substrate-imprinted symmetry inhibits predicted Ti displacement proper ferroelectricity, and, instead, phonon softening critical to ferroelectric order emerges at low temperatures. Confined within the (110) plane, there exists significant orbital distortion instigated through the O_h oxygen displacement

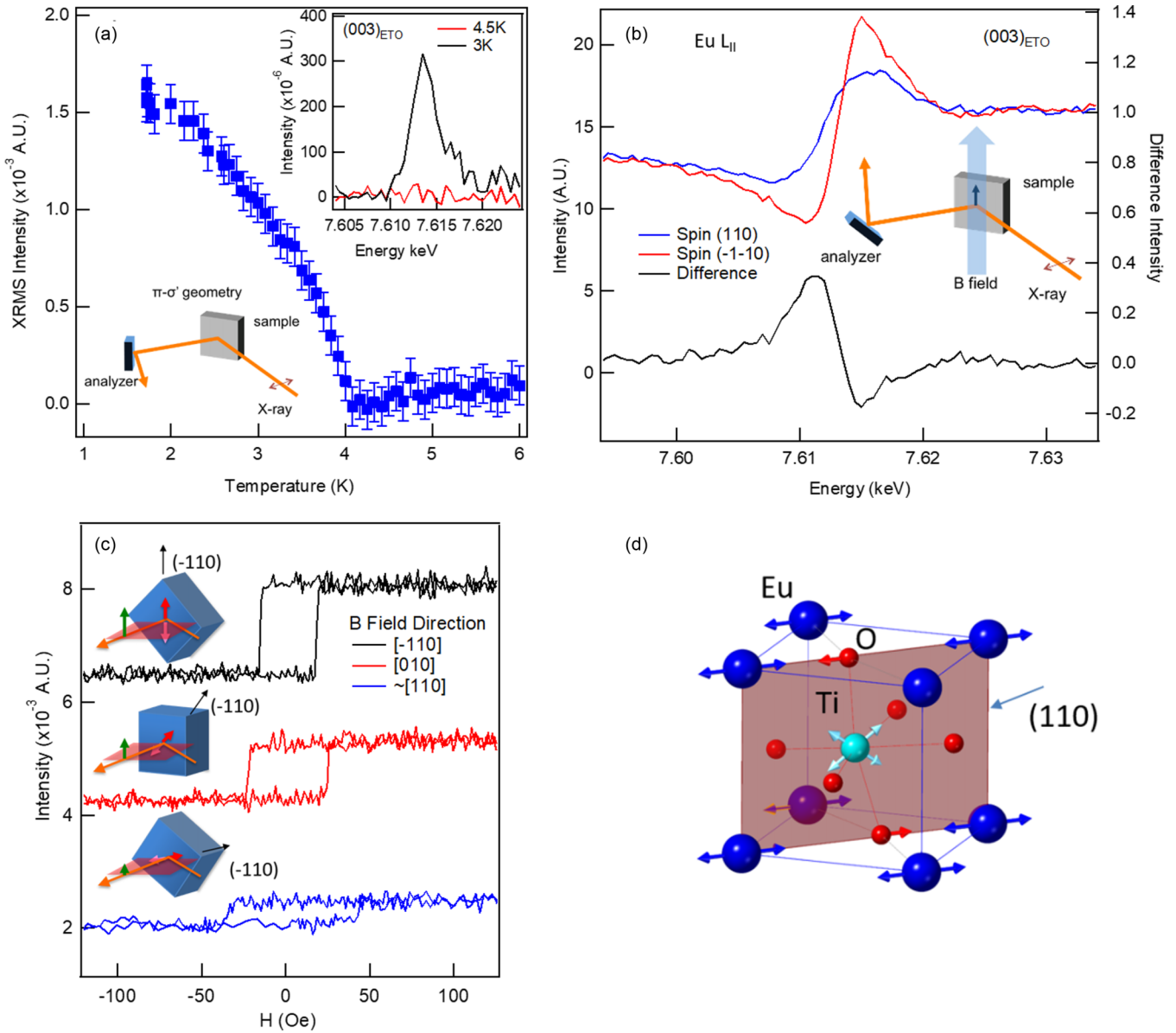


FIG. 3. (a) Temperature-dependent XRMS-scattering intensity of the $(003)_{\text{ETO}}$ reflection at the $\text{Eu } L_{\text{II}}$ edge indicative of FM spin order. The inset of the bottom left corner illustrates the horizontal-scattering experimental configuration (π - σ), and the top right shows resonant enhancement (background subtracted) above and below T_c . (b) Energy scans at the $(003)_{\text{ETO}}$ reflection in (π - π) geometry where the charge-scattering intensity can interfere with the magnetic scattering. The in- and out-of-phase interferences of magnetic and charge scatterings are dependent on the aligned spin direction. (c) Field-dependent sweeps with fixed energy in (π - π) showing clear FM hysteresis loops. Data are offset for clarity. With the applied field along the easy magnetic axis $[\bar{1}10]$, the hysteresis loop shows a minimum coercivity. Along the $[010]$ and close to the $[110]$, the intensity difference between positive and negative field directions decreases, and the loop broadens. The inset images illustrate, regardless of changes in the field direction by sample rotation, the spins stay within the easy axis $[\bar{1}10]$. (d) A cartoon model illustrating the relative orientation of the oxygen O_h tilting, Ti phonon softening, and uniaxial magnetic anisotropy.

shaping both the Ti phonon landscape and the Eu $4f$ orbitals. Hybridization between Ti $3d$ and Eu $4f$ states facilitates the effective charge transfer (sharing) between the two, leading to expected ferroelectric order suppression. The single oxygen octahedral tilt domain fortuitously creates an ideal opportunity to study the underlying nature of how spin, lattice, orbital, and charge order parameters couple. In doing so, we show how the $4f$ spin structure is set by interorbital shaping as determined by intricately entangled order parameters confined

ultimately by symmetry. Our findings will provide guidance in varying external tuning parameters to study multiferroic quantum criticality in ETO-related systems.

Work at Argonne and the use of beamline 6-ID-B at the Advanced Photon Source at Argonne was supported by the U. S. Department of Energy, Office of Science, Office of Basic Energy Sciences under Contract No. DE-AC02-06CH11357. The EPSRC-funded XMaS beamline at the

ESRF is directed by M. J. Cooper, C. A. Lucas, and T. P. A. Hase. We are grateful to O. Bikondoa, D. Wermeille, and L. Bouchenoire for their invaluable assistance and to S. Beaufoy and J. Kervin for additional XMaS support. The work at Cornell was supported by the U.S. Department of Energy, Office of Basic Energy Sciences, Division of Materials Sciences and Engineering under Award No. DE-SC0002334. Substrate preparation was performed, in part, at the Cornell NanoScale Facility, a member of the National Nanotechnology Coordinated Infrastructure (NNCI), which

is supported by the National Science Foundation (Grant No. NNCI-1542081). Use of beamline X23-A2 at the National Synchrotron Light Source was supported by the U.S. Department of Energy, Office of Basic Energy Sciences under Contract No. DE-AC02-98CH10886. Additional support was provided by the National Institute of Standards and Technology. The work at the University of Minnesota was funded by the Department of Energy through the University of Minnesota Center for Quantum Materials under Grant No. DE-SC-0016371.

-
- [1] M. Fiebig, *J. Phys. D: Appl. Phys.* **38**, R123 (2005).
- [2] W. Eerenstein, N. D. Mathur, and J. F. Scott, *Nature (London)* **442**, 759 (2006).
- [3] A. Narayan, A. Cano, A. V. Balatsky, and N. Spaldin, *Nat. Mater.* **18**, 223 (2019).
- [4] T. Katsufuji and H. Takagi, *Phys. Rev. B* **64**, 054415 (2001).
- [5] T. R. McGuire, M. W. Shafer, R. J. Joenk, H. A. Alperin, and S. J. Pickart, *J. Appl. Phys.* **37**, 981 (1966).
- [6] T. Birol and C. J. Fennie, *Phys. Rev. B* **88**, 094103 (2013).
- [7] C. J. Fennie and K. M. Rabe, *Phys. Rev. Lett.* **97**, 267602 (2006).
- [8] J. H. Lee, L. Fang, E. Vlahos, X. Ke, Y. Woo Jung, L. F. Kourkoutis, J.-W. Kim, P. J. Ryan, T. Heeg, M. Roeckerath, V. Goian, M. Bernhagen, R. Uecker, P. C. Hammel, K. M. Rabe, S. Kamba, J. Schubert, J. W. Freeland, D. A. Muller, C. J. Fennie, P. Schiffer, V. Gopalan, E. Johnston-Halperin, and D. G. Schlom, *Nature (London)* **466**, 954 (2010).
- [9] N. Das, *Phys. Lett. A* **376**, 2683 (2012).
- [10] X. Ke, T. Birol, R. Misra, J.-H. Lee, B. J. Kirby, D. G. Schlom, C. J. Fennie, and J. W. Freeland, *Phys. Rev. B* **88**, 094434 (2013).
- [11] N. A. Benedek and C. J. Fennie, *J. Phys. Chem. C* **117**, 13339 (2013).
- [12] S. J. May, J.-W. Kim, J. M. Rondinelli, E. Karapetrova, N. A. Spaldin, A. Bhattacharya, and P. J. Ryan, *Phys. Rev. B* **82**, 014110 (2010).
- [13] P. Ryan, J. W. Kim, T. Birol, P. Thompson, J.-H. Lee, X. Ke, P. Normile, E. Karapetrova, P. Schiffer, S. Brown, C. Fennie, and D. Schlom, *Nat. Commun.* **4**, 1334 (2013).
- [14] R. Cohen, *Nature (London)* **358**, 136 (1992).
- [15] H. Akamatsu, Y. Kumagai, F. Oba, K. Fujita, H. Murakami, K. Tanaka, and I. Tanaka, *Phys. Rev. B* **83**, 214421 (2011).
- [16] R. V. Vedrinskii, V. L. Kraizman, A. A. Novakovich, P. V. Demekhin, and S. V. Urazhdin, *J. Phys.: Condens. Matter* **10**, 9561 (1998).
- [17] J. C. Woicik, E. L. Shirley, C. S. Hellberg, K. E. Andersen, S. Sambasivan, D. A. Fischer, B. D. Chapman, E. A. Stern, P. Ryan, D. L. Ederer, and H. Li, *Phys. Rev. B* **75**, 140103(R) (2007).
- [18] E. A. Stern, *Phys. Rev. Lett.* **93**, 037601 (2004).
- [19] D. Manuel, D. Caberet, C. Brouder, P. Sainctavit, A. Bordage, and N. Trcera, *Phys. Rev. B* **85**, 224108 (2012).
- [20] R. F. Berger, C. J. Fennie, and J. B. Neaton, *Phys. Rev. Lett.* **107**, 146804 (2011).
- [21] R. A. Wheeler, M.-H. Whangbo, T. Hughbanks, R. Hoffman, J. K. Burdett, and T. Albright, *J. Am. Chem. Soc.* **108**, 2222 (1986).
- [22] D. J. Singh, M. Ghita, M. Fornari, and S. V. Halilov, *Ferroelectrics* **338**, 73 (2006).
- [23] N. Hill, *J. Phys. Chem. B* **104**, 6694 (2000).
- [24] W. Zhong and D. Vanderbilt, *Phys. Rev. Lett.* **74**, 2587 (1995).
- [25] P. M. Woodward, *Acta Crystallogr. Sect. B: Struct. Sci.* **53**, 44 (1997).
- [26] H. Akamatsu, Y. Kumagai, F. Oba, K. Fujita, K. Tanaka, and I. Tanaka, *Adv. Funct. Mater.* **23**, 1864 (2013).
- [27] C. J. Howard and H. T. Stokes, *Acta Crystallogr., Sect. B: Struct. Crystallogr. Cryst. Chem.* **54**, 782 (1999).
- [28] T. H. Kim, D. Puggioni, Y. Yuan, L. Xie, H. Zhou, N. Campbell, P. J. Ryan, Y. Choi, J.-W. Kim, J. R. Patzner, S. Ryn, J. P. Podkaminer, J. Irwin, Y. Ma, C. J. Fennie, M. S. Rzechowski, X. Q. Pan, V. Gopalan, J. M. Rondinelli, and C. B. Eom, *Nature (London)* **533**, 68 (2016).
- [29] D. Bessas, K. Z. Rushchanskii, M. Kachlik, S. Disch, O. Gourdon, J. Bednarcik, K. Maca, I. Sergueev, S. Kamba, M. Lezaic, and R. P. Hermann, *Phys. Rev. B* **88**, 144308 (2013).
- [30] Y. Yang, W. Ren, D. Wang, and L. Bellaiche, *Phys. Rev. Lett.* **109**, 267602 (2012).
- [31] J.-W. Kim, P. Thompson, S. Brown, P. S. Normile, J. A. Schlueter, A. Shkabko, A. Weidenkaff, and P. J. Ryan, *Phys. Rev. Lett.* **110**, 027201 (2013).
- [32] R. Ranjan, H. Sadat Nabi, and R. Pentcheva, *J. Phys.: Condens. Matter* **19**, 406217 (2007).
- [33] D. Hupfeld, O. H. Seeck, J. Voigt, J. Bos, K. Fischer, and T. Brückel, *Europhys. Lett.* **59**, 284 (2002).
- [34] M. Blume, *J. Appl. Phys.* **57**, 3615 (1985).